ACS APPLIED MATERIALS & INTERFACES

Research Article

Cite This: ACS Appl. Mater. Interfaces 2018, 10, 42198−42206

www.acsami.org

Ion-Selective Polyamide Acid Nanofiber Separators for High-Rate and Stable Lithium−Sulfur Batteries

Xiang Luo,[†] Xianbo Lu,[‡] Gangyong Zhou,[†] Xingyu Zhao,[†] Yue Ouyang,[†] Xiaobo Zhu,[†] Yue-E Miao,*[,†] and Tianxi Liu[†]

[†]State Key Laboratory for Modification of Chemical Fibers and Polymer Materials, College of Materials Science and Engineering, Innovation Center for Textile Science and Technology, Donghua University, 2999 North Renmin Road, Shanghai 201620, P. R. China

[‡]R&D Center, Shanghai Kingfa Science & Technology Co., Ltd., 88 Kangyuan Road, Shanghai 201714, P. R. China

Supporting Information

ABSTRACT: Lithium−sulfur (Li−S) batteries have attracted great attention because of their high energy density and high theoretical capacity. However, the "shuttle effect" caused by the dissolution of polysulfides in liquid electrolytes severely hinders their practical applications. Herein, we originally propose a carboxyl functional polyamide acid (PAA) nanofiber separator with dual functions for inhibiting polysulfide transfer and promoting Li^+ migration via a one-step electrospinning synthesis method. Especially, the functional groups of −COOH in PAA separators provide an electronegative environment, which promotes the transport of Li^+ but suppresses the migration of negative polysulfide anions. Therefore, the PAA nanofiber separator can act as an efficient electrostatic shield to restrict the polysulfide on the cathode side, while efficiently promoting Li^+ transfer across the separator. As a result, an ultralow decay rate of only 0.12% per cycle is achieved for the PAA nanofiber separator after 200 cycles at 0.2 C, which is less than half that (0.26% per cycle) of the commercial Celgard separator.

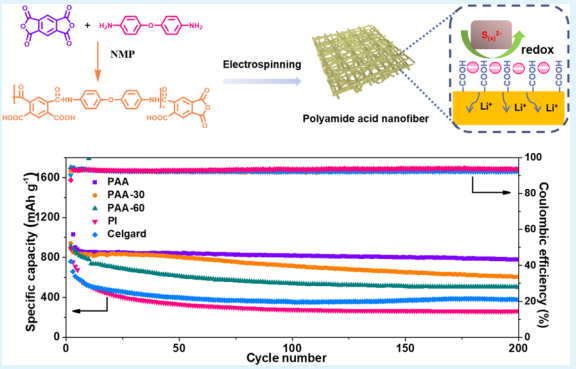

KEYWORDS: *electrospun nanofibers, ion selective, dual functions, separator, lithium−sulfur battery*

1. INTRODUCTION

In order to meet the ever-increasing demand for high-energy-density batteries, advanced energy storage systems are highly desired.[1] Recently, lithium−sulfur (Li−S) batteries have drawn wide attention because of their high theoretical energy density of 2600 W h kg^{-1} and high safety features compared to the currently commercialized lithium-ion batteries.[2] However, one critical problem is the "shuttle effect", which is caused by the easy diffusion of high-order polysulfides from the sulfur cathode to the lithium anode side. The high-order polysulfide reacts with metal lithium to form a low-order polysulfide, which then diffuses back to the cathode side circularly. Thus, the shuttle effect finally results in the low Coulombic efficiency, loss of the active materials, as well as poor cycle stability.[3−5]

As is known, the separator is one important component in a battery system, which provides the function of separating the cathode and anode to prevent short circuit but allows the transport of Li^+ through the membranes. However, polysulfides can easily pass across the conventional separators and react with the lithium metal, leading to battery life attenuation. In order to prevent the "shuttle effect" of polysulfides, many studies have been reported in the exploitation of functional separators, such as coating the Celgard separators by carbon materials,[6−9] functional polymers,[10−12] inorganic materials, and so on.[13−16] While inhibiting the polysulfide transport, these methods also impede the migration of Li^+.

The cation-selective membranes have been considered to possess unique function of separating cations and anions in solution. When a cation-selective membrane is used as the separator for the Li−S cell, the "shuttle effect" of polysulfides will be fully suppressed. Besides, the cation-selective membrane will be beneficial for promoting the transport rate of Li^+ through the Coulombic interactions. For example, Wei's group introduced a cation-permselective membrane with $-SO_3^-$ groups acting as an electrostatic shield for polysulfide anions, which largely improved the performance of the Li−S battery.[17] Yang and co-workers further studied the interaction between $-SO_3^-$ groups and polysulfides by theoretical calculations. They found that the sulfonic group acts as an ion-selective group weakening the transfer of electronegative ions (polysulfide) but promotes the transport of Li^+ as well as absorbs part of the polysulfide through the Li−O bond.[18] Like

Received: June 28, 2018
Accepted: October 30, 2018
Published: October 30, 2018

DOI: 10.1021/acsami.8b10795
ACS Appl. Mater. Interfaces 2018, 10, 42198−42206

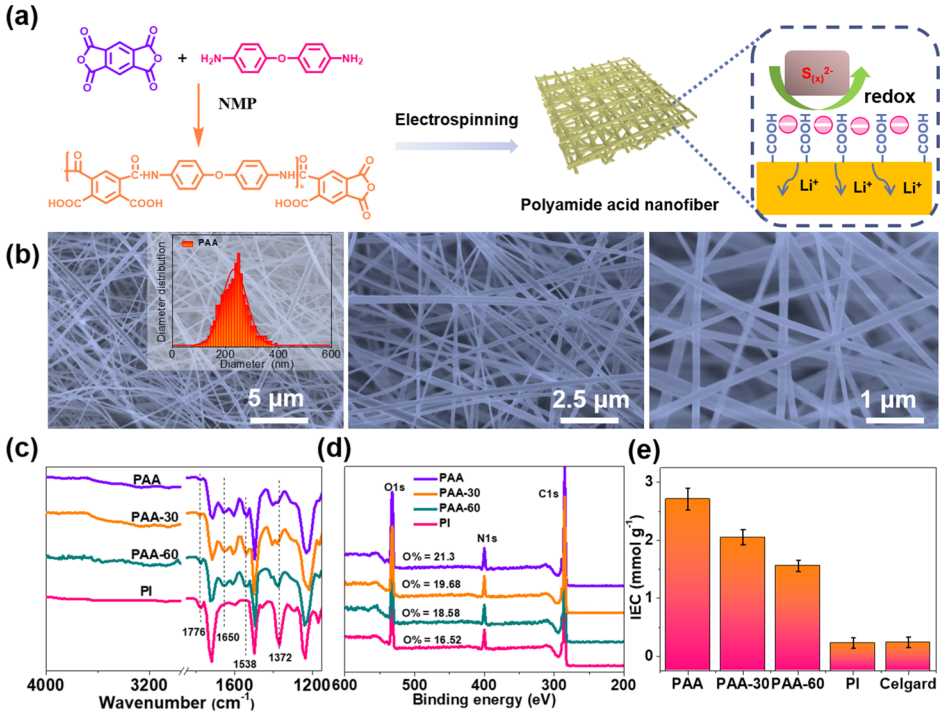

Figure 1. (a) Schematic illustration of the preparation process of the PAA nanofiber separator. (b) SEM images of the PAA separator at different magnifications. (c) FTIR and (d) XPS spectra of PAA separators with different amounts of carboxyl groups. (e) IEC values for different separators.

$-SO_3^-$ groups, the −COOH group, another kind of ion-selective groups which possesses unshared electron pairs, has the ability of interacting with Li^+ in the solvent and promotes the transfer rate of Li^+.[19] It has been reported that the introduction of −COOH groups in the separator could significantly affect the electrochemical behavior, especially to improve the Li^+ transport properties.

On the other hand, polyimide (PI) is one of the organic polymers, which possesses the best comprehensive properties such as excellent chemical stability, high thermal decomposition temperature (around 500 °C), good mechanical properties, and so on.[20,21] To take advantage of its excellent properties, many kinds of PI-based separators have been prepared by electrospinning or phase inversion approaches to apply as a separator matrix for lithium-ion batteries.[19,22−24] Actually, the precursor of PI, polyamide acid (PAA), is a class of polymers with abundant −COOH groups. Herein, we present a specially designed carboxyl functional PAA nanofiber separator with dual functions to simultaneously inhibit polysulfide transfer and promote Li^+ migration via a facile electrospinning strategy. Compared with the previously reported carbon material-modified separators, the PAA nanofiber separator can not only effectively inhibit the shuttle effect of polysulfides but also promote the diffusion of Li^+. Besides, the PAA separator possesses good thermal stability, high porosity, outstanding electrolyte wettability, and remarkable electrolyte uptake. Finally, the Li−S battery assembled with the PAA nanofiber separator exhibits a high initial discharge capacity of 1031 mA h g^{-1} at 0.2 C, a remarkable rate capability of 408 mA h g^{-1} at 5 C, and a good capacity retention of 781.8 mA h g^{-1} (76%) after 200 cycles at 0.2 C, being promising as a competitive candidate for the commercial Celgard separator in Li−S battery applications.

2. EXPERIMENTAL SECTION

2.1. Materials. 4,4′-Oxydiamine (ODA) and pyromellitic dianhydride (PMDA) (Sigma-Aldrich) were purified by recrystallization before use. *N*,*N*-Methyl pyrrolidone (NMP) (Shanghai Chemistry Company) was purified by distillation before use.

2.2. Preparation of PAA Nanofiber Separators. The PAA nanofiber membrane was prepared by the following two steps (Figure 1a). First, ODA (3.962 g, 0.018 mol) was completely dissolved in 100 mL NMP. Then, PMDA (4.425 g, 0.02 mol) was added into the NMP solution little by little under strong mechanical stirring at 0 °C in N_2 atmosphere for 4 h to obtain the PAA solution. After that, the electrospinning process was conducted to get the PAA nanofiber membranes with a thickness of around 35 μm. The applied voltage is 17−24 kV, and the diameter of the spinning nozzle is 0.5 mm. Then, the membranes were dried overnight at 70 °C for 24 h. Finally, the membrane was imidized in an oven at 200 °C for different times (0, 30, 60, and 180 min, respectively) to obtain PAA nanofiber membranes with different amounts of carboxyl groups, which were named as PAA, PAA-30, PAA-60, and PAA-180 (i.e., PI), respectively.

2.3. Characterizations. The chemical composition of the separators was analyzed by Fourier transform infrared (FTIR, Bruker Co., Germany) and X-ray photoelectron spectroscopy (XPS PHI 5000C ESCA system, PHI Co., USA). The microstructure of the separators was studied by a scanning electron microscope (Tescan). Thermogravimetric analysis (Pyris 1 TGA) was conducted under nitrogen atmosphere from 30 to 900 °C with a heating rate of 20 °C min^{-1}. The wettability of separators to the liquid electrolyte was characterized by contact angle (Dataphysics OCA40 Micro). The porosity and electrolyte uptakes of the separators were characterized according to the literature.[25,26] The ionic exchange capacity (IEC, mmol g^{-1}) was tested by acid−base titration. The separators were soaked into 3 mol L^{-1} sodium chloride solution for 8 h to deprotonate. Then, the separators were taken out, and the solution was titrated with 0.1 mol L^{-1} sodium hydroxide solution. Finally, the IEC was calculated according to the following equation:[19] IEC = $(\Delta V_{NaOH} \times C_{NaOH})/W_s$, where ΔV_{NaOH} is the volume of sodium hydroxide solution used in titration, C_{NaOH} is the molar concentration of sodium hydroxide solution, and W_s is the weight of the dried separator.

DOI: 10.1021/acsami.8b10795
ACS Appl. Mater. Interfaces 2018, 10, 42198−42206

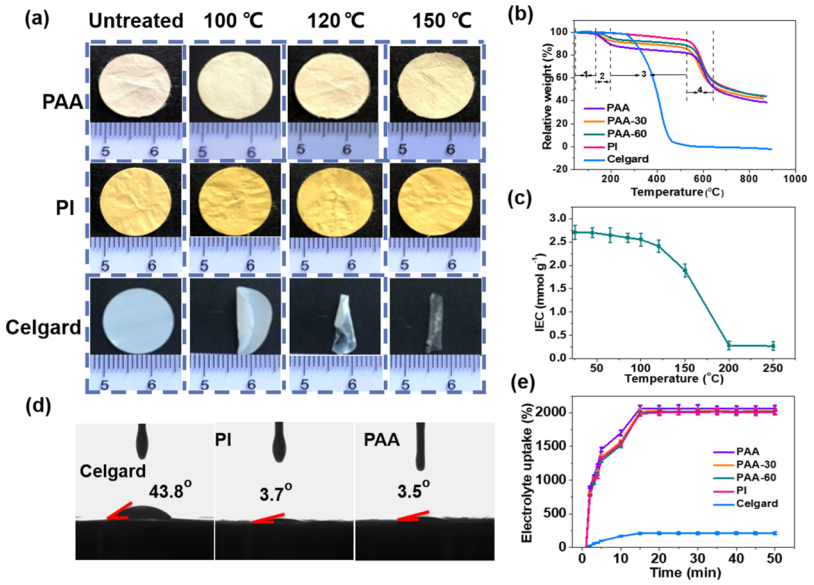

Figure 2. (a) Thermal shrinkage and (b) TGA curves of different separators. (c) IEC values of the PAA separator at different temperatures; (d) contact angles, and (e) electrolyte uptakes of PAA, PI, and Celgard separators.

2.4. Electrochemical Measurements. Sulfur electrodes were fabricated by pasting the sulfur slurry [including 65 wt % sulfur as the active material, 30 wt % super P, and 5 wt % poly(vinylidene difluoride) binder] onto the aluminum foil current collector. The slurry pasted Al foils were vacuum-dried at 60 °C overnight. Then, the sulfur electrodes with the sulfur loading of 2.2 mg cm^{-2} were cut into circular pellets and used as the working electrodes. The coin cell (CR2032) was assembled in an argon-filled glovebox, and the amount of electrolyte used was 70 μL.

The galvanostatic discharge/charge properties of the cells were carried out on a LAND CT2001A system with the potential of 1.7−2.8 V. The Li^+-transfer number for different separators was characterized by chronoamperometry according to the literature.[27]

The electrochemical impedance spectroscopy (EIS) measurement was conducted on the CHI660E electrochemical working station. The ionic conductivity of the separators was calculated from the EIS result.[28]

The electrochemical window of the separators was evaluated by the linear sweep voltammetry test with the potential of 1.0−7.0 V.

3. RESULTS AND DISCUSSION

3.1. Structures and Morphologies of the Separators. The morphologies of PAA and PI separators were observed by scanning electron microscopy (SEM). It can be seen in Figures 1b and S1 that the diameter of both PAA and PI nanofibers is about 250 nm and the distribution is relatively uniform, which is quiet important to maintain the stability of the batteries during discharge and charge.

FTIR was used to verify the structural difference between the separators. From Figure 1c, it can be seen that the absorption band at about 1650 cm^{-1} is ascribed to amide I of carbonyl stretching and the band at 1538 cm^{-1} is ascribed to amide II of N−H bending. However, with increasing imidization time, these two peaks weaken gradually and disappear in the PI separator. At the same time, the absorption peak of O−H is around 3000−3700 cm^{-1}, which weakens as well and disappears in the PI separator, indicating that all −COOH groups are involved in the imidization reactions. Moreover, imide I (1776 cm^{-1}) and imide II (1372 cm^{-1}) of carbonyl stretching are strengthened in the PI separator, which are basically in accordance with the imidization reaction consumption of the imide groups.[29] XPS was further used to demonstrate the imidization reaction of the PAA separators. Figure 1d indicates an obvious decrease in the oxygen content, corresponding to the consumption of −COOH groups during the imidization reactions. The definite content of the −COOH groups in the PAA separators is determined by the IEC values of the separators. According to Figure 1e, the IEC values of the PAA separators decrease with the increasing reaction degree of the imine groups.

The thermal stability of the separators was characterized through tracing the thermal contraction of the separators at different temperatures. The three kinds of separators (i.e., PAA, PI, and commercial Celgard) were deposited at different temperatures for 0.5 h. As displayed in Figure 2a, no apparent thermal contraction occurs below 100 °C. When increasing the temperature, both PAA and PI separators show no change with an excellent thermal stability. In contrast, the Celgard separator shows a drop in size at 100 °C. This is attributed to the coaxial stretching process of the Celgard separator. When the temperature is increased over 120 °C, the Celgard separator shrinks and curls severely. The dramatic difference implies that PAA and PI have a superior thermal stability over that of the Celgard separator, which could make contributions to enhance the safety of high-power L−S batteries. However, the color of the PAA separator changes slightly when the treatment temperature is 150 °C, possibly due to a partial imidization reaction.

TGA was further carried out as shown in Figure 2b. It can be observed that the weight loss of PAA can be divided into four steps. From the room temperature to 120 °C (stage 1), the weight loss is about 2 wt %, which can be ascribed to the volatilization of the residual solvent. The weight loss of the second stage (120−250 °C) is ascribed to the water escape during the imidization reaction of PAA. During the third stage from 250 to 500 °C, a wide temperature range indicates the excellent thermal stability of PI. The weight loss in the last stage (above 500 °C) is attributed to the degradation of PI. From the TGA curves of PAA, PAA-30, PAA-60, and PI, it can also be seen that the weight loss during the second stage

DOI: 10.1021/acsami.8b10795
ACS Appl. Mater. Interfaces 2018, 10, 42198−42206

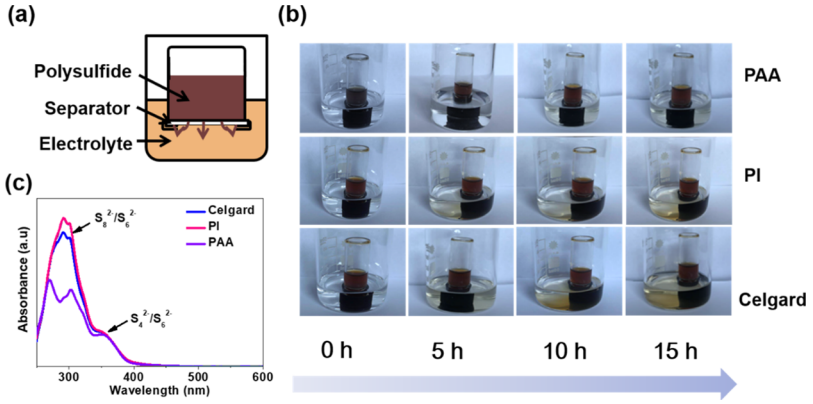

Figure 3. Polysulfide diffusion measurements: (a) diagram of the diffusion test bottle showing the polysulfide solution, separator, and blank electrolyte. The above bottle was immersed into the blank electrolyte, and the concentration of polysulfide that permeated the separator was supervised by UV−vis spectroscopy. (b) Photographs of polysulfide permeation across the PAA, PI, and Celgard separators for standing times of 0, 5, 10, and 15 h, respectively. (c) UV−vis spectra of polysulfide solutions after 15 h, indicating the superior performance of the PAA separator.

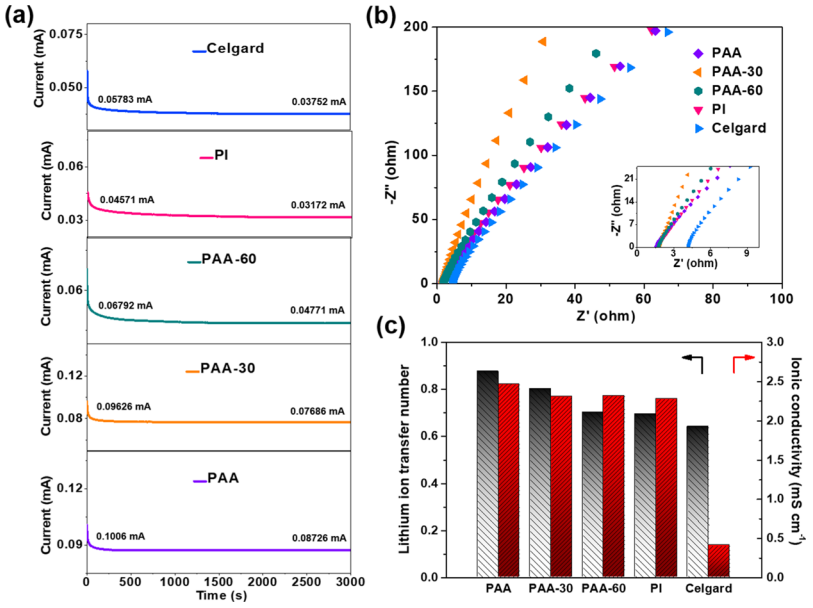

Figure 4. (a) Chronoamperometry profiles and (b) impedance plots estimating Li^+ conductivity for different separators. (c) Li^+-transfer number and the ionic conductivity for different separators.

decreases with increasing thermal treatment time, implying a gradual imidization process during the heat treatment. The effect of temperature on the IEC value of PAA was also studied at different temperatures for 30 min (Figure 2c). Obviously, the IEC value decreases with increasing heating temperature. Furthermore, when the temperature reaches 200 °C, the IEC value is close to zero, indicating a completed imidization process above 200 °C.

Porosity of the separator is also considered as an important factor affecting the battery performance. Benefitting from the well-distributed porous structure of the nanofibers, the porosities of PAA (92.2%), PAA-30 (92.1%), PAA-60 (92%), and PI (92.1%) separators are much higher than that of Celgard (41.6%) according to the tests by a liquid absorption method (Table S1). Besides, the affinity of the separator to liquid electrolyte is also very important to determine the performance of the L−S batteries, which was detected by the contact angle testing. The results are shown in Figure 2d, with the liquid electrolyte contact angles of 43.8°, 3.7°, and 3.5° for Celgard, PI, and PAA separators, respectively. The significant decrease of the contact angle for PI separator is due to the much close polarity between PI nanofiber-based nonwoven separators and the highly polar liquid electrolyte. The further increased polarity of PAA is reflected from its much higher adsorption rate to the electrolyte. Hence, the PAA, PAA-30, PAA-60, and PI separators are more quickly wetted with higher electrolyte uptakes of 2065, 2058, 2049, and 2010%, respectively (Figure 2e), as compared to the Celgard separator (210%). Moreover, the electrolyte uptake increases slightly with an increase in the content of the highly polar −COOH groups in PAA-based nanofiber separators.

To verify the efficiency of polysulfide trapping by the PAA-based separators, polysulfide diffusion tests were conducted as shown in Figure 3a,b. Three different cases with PAA, PI, and Celgard separators are tested, respectively. As for Celgard and PI separators, polysulfide easily diffuses across the separators into the originally colorless blank electrolyte. Conversely, the presence of a PAA separator makes the diffusion of polysulfide much slower. Figure 3c is the UV curves of the electrolyte obtained after diffusion for 10 h, and the peak at 290 nm

DOI: 10.1021/acsami.8b10795
ACS Appl. Mater. Interfaces 2018, 10, 42198−42206

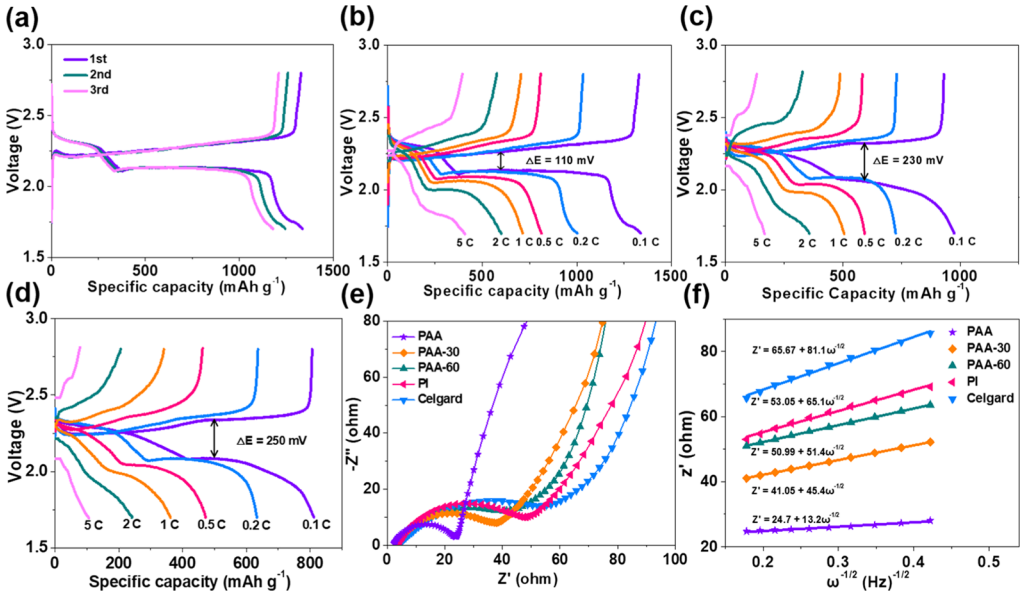

Figure 5. (a) Discharge/charge profiles of the battery with the PAA separator at the first three cycles. The discharge/charge profiles of Li−S batteries with (b) PAA, (c) PI, and (d) Celgard separators at different C rates. (e) Nyquist plots and (f) relationship between Z' and $\omega^{-1/2}$ in the low-frequency region of cells with different separators.

represents S_8^{2-} and S_6^{2-}.[30−32] It is obvious that the absorbance intensity of polysulfide solutions obtained by diffusion through the PAA separator is the weakest among the three cases, further confirming that the PAA separator can efficiently inhibit polysulfide diffusion by Coulombic interactions between −COOH groups and polysulfide anions.

3.2. Electrochemical Performances. For the sake of ensuring the influence of the −COOH groups on the Li^+ transport properties, both the Li^+-transfer number and ionic conductivity were detected by chronoamperometry profiles (Figure 4a) and EIS (Figure 4b). Compared with the other four separators, the PAA separator possesses a much higher Li^+-transfer number of 0.86 (Figure 4c) according to the chronoamperometry profiles, which is also a much higher value compared to those of the previously reported separators (Figure S2).

The ionic conductivities of the separators were analyzed by EIS. It can be seen that the bulk resistances (R_b) of the PAA, PAA-30, PAA-60, PI, and Celgard separators are 1.58, 1.76, 1.83, 1.85, and 4.19 Ω, respectively (Figure 4b). Consequently, the calculated ionic conductivities of PAA-based separators are much higher than that of the Celgard separator (Figure 4c). The high Li^+-transfer number and outstanding ionic conductivity can be ascribed to two reasons. First, because of the strong polarity caused by a large number of carboxyl groups, the PAA-based membrane could fix more electrolytes, which will largely facilitate the flow rate of Li^+ across the pores of the PAA-based separators. Second, the −COOH groups can provide an electronegative atmosphere and further accelerate the transport of Li^+. Besides, the higher porosity of PAA-based separators can also afford much more channels for ion migration.

Figure 5a presents the discharge/charge profiles of the PAA separator at a current density of 0.2 C (1 C = 1675 mA g^{-1}). The typical two-plateau phenomena of a Li−S system are observed at around 2.3 and 2.1 V in the discharge curve, indicating the particular multielectron redox reactions and phase transformations of long-chain polysulfide (from elemental sulfur to dissolved Li_2S_n) and short-chain polysulfide (from dissolved Li_2S_n to insoluble Li_2S_2 or Li_2S).[4,5,33] The discharge/charge curves of the cells with PAA, PI, and Celgard separators are further conducted at various C rates. As exhibited in Figure 5b−d, the overvoltage (ΔE) of cells with the PAA separator (110 mV) is much smaller than those of PI (230 mV) and Celgard (250 mV) separators, which indicates the lower polarization and better round-trip energy efficiency of the PAA separator. At a current density of 0.1 C, the discharge specific capacity of the PAA separator reaches 1334 mA h g^{-1}. Even though the current density is as high as 5 C, the cell with the PAA separator still maintains the ∼2.0 V discharge plateau with a high specific capacity of 408 mA h g^{-1}, demonstrating an excellent rate performance.

EIS is an effective method to study the diffusion coefficient of Li^+.[34] As shown in Figure 5e, the semicircle part of the EIS curves represents the contact resistance and the value of resistance (R_{ct}) related to Li^+-transfer properties. It is obvious that the batteries using PAA, PAA-30, PAA-60, and PI separators have considerably lower bulk resistances of 24, 38, 45, and 48 Ω, respectively, compared to that of Celgard (55 Ω), suggesting a faster Li^+ diffusion rate. Besides, the bulk resistance decreases with an increase in the content of −COOH groups, which is consistent with the previous reports.[34] That is, the interfacial resistance always decreases after the polar modification is introduced in the separator. The different charge-transfer resistances between PAA, PI, and Celgard separators could be mainly attributed to their different molecular structures. The PAA separator with polar −COOH groups is good for the permeation of the separators by the electrolyte, which will facilitate the transport of Li^+ and lead to a decreased resistance. Furthermore, with an increase in the number of −COOH groups, the bulk resistivity decreases. It indicates that the existence of −COOH groups significantly improved the electrode/electrolyte interaction. Figure 5f shows the linear fittings of Z', where ω is the angular frequency. By comparing the slopes of the fitting lines, namely, the Warburg factor that determines the Li^+ diffusion coefficient value,[35] it

DOI: 10.1021/acsami.8b10795
ACS Appl. Mater. Interfaces 2018, 10, 42198−42206

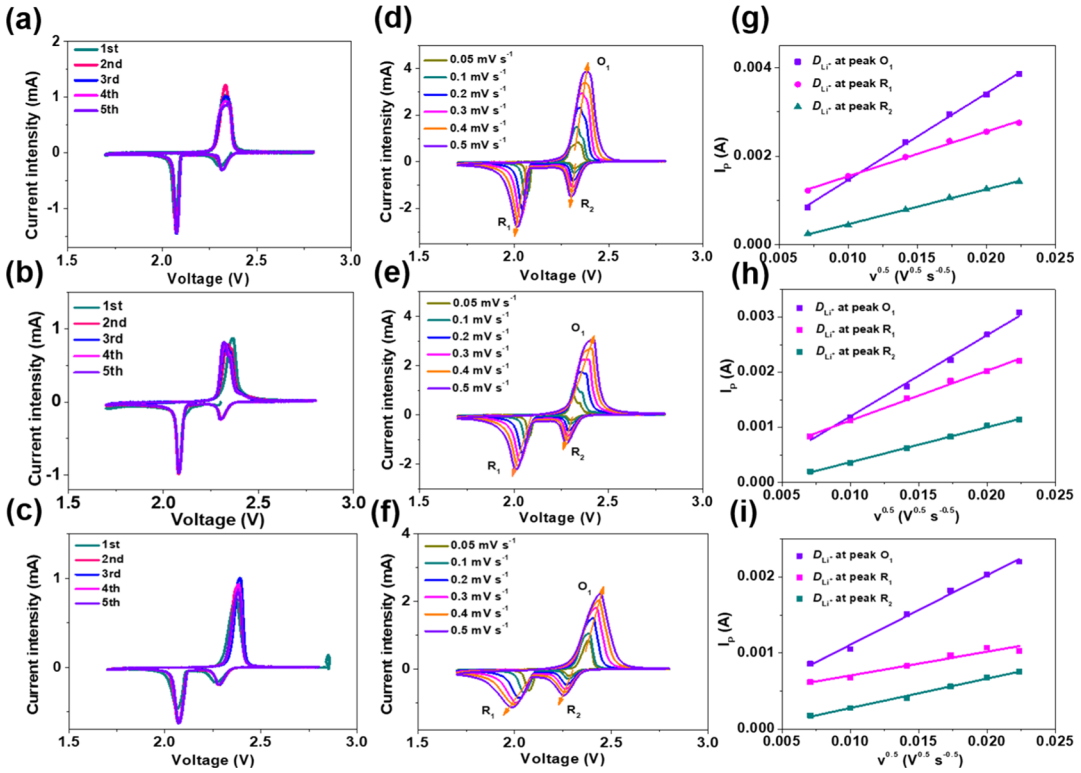

Figure 6. CV curves of first five cycles (a–c), CV curves at various voltage scan rates (d–f), as well as the corresponding linear fits of the peak currents (g–i) of Li–S batteries with PAA, PI, and Celgard separators, respectively.

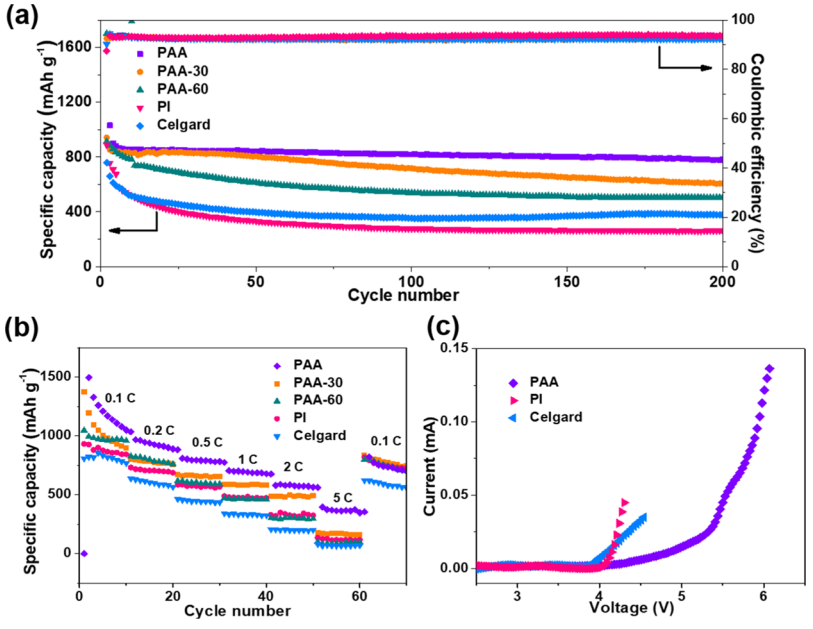

Figure 7. (a) Cycle performance, (b) rate capability, and (c) *I*–*V* curves of the cells assembled with PAA, PI, and Celgard separators.

indicates that the PAA separator has the highest Li^+ diffusion coefficient among all of the separators.

The cyclic voltammetry (CV) curves of the first five cycles for the batteries assembled with PAA, PI, and Celgard separators are presented in Figure 6a–c. The scan rate is 0.1 mV s^{-1}, and the range of voltage is 1.7–2.8 V. Two characteristic peaks on the reduction scan at around 2.3 and 2.0 V can be observed, representing the transformation of elemental sulfur to soluble polysulfide (Li_2S_n, $4 < n < 8$) and then changes into solid lithium sulfides (Li_2S_2/Li_2S), respectively.[36] In the curve of anodic scan, one oxidation peak at about 2.5 V is discerned, which corresponds to the conversion of polysulfide to elemental sulfur. The highly consistent overlaps of the cathodic and anodic peaks of the PAA separator, compared to those of PI and Celgard separators, indicate that the battery assembled with the PAA separator is highly stable.[6] Furthermore, the Li^+ diffusion coefficients (D_{Li^+}) of the separators were also counted by a

DOI: 10.1021/acsami.8b10795
ACS Appl. Mater. Interfaces 2018, 10, 42198–42206

range of CVs.[37] As summarized in Table S2, the D_{Li^+} for cells with the PI separator increases compared to those with the Celgard separator because of the high porosity of the PI separator. For the PAA separator, further increased Li^+ diffusion coefficients are obtained, which is possibly because of the largely promoted ion transport of positively charged Li^+ by Coulombic interactions between the negatively charged −COOH groups and Li^+.

Figure 7a shows the cycling performance of the cells with different separators at a current density of 0.2 C for 200 cycles. At the first cycle, PAA, PAA-30, PAA-60, PI, and Celgard cells deliver specific capacities of 1031, 941, 912, 887, and 758 mA h g^{-1}, respectively. It is obvious that the cells with PAA, PAA-30, PAA-60, and PI separators show higher capacities than Celgard, which can be attributed to the high porosity and high electrolyte uptake of electrospun nanofiber membranes. During the ongoing cycles, the capacities of the cells with PI and Celgard separators decrease significantly with very low retentions of 29.5 and 49.9% after 200 cycles, respectively. The lower capacity retention of the cell with the PI separator might be caused by the large pore size of the electrospun nanofiber separator, which makes the transport of polysulfides much easier. On the other hand, the capacity of the cell with the PAA separator decreases slightly with 76% retention after 200 cycles, corresponding to an ultralow decay rate of 0.12% per cycle. Besides, from the results of energy-dispersive X-ray spectroscopy (EDS) elemental mapping (Figure S3), it can be observed that the sulfur element is evenly distributed over the entire cathode electrode before and after cycle with little decrease, indicating that the PAA separator can efficiently inhibit the "shuttle effect" of polysulfides and prevent the loss of the active material. The much better cycling stability of the PAA separator is supposed to be derived from the −COOH groups in the polymer chains of PAA, which can significantly reject the transport of polysulfide (S_n^{2-}) through Coulombic interactions and improve the cycling stability of Li−S batteries.

The rate performances of the separators were studied under different current densities (Figure 7b). The cell with the PAA separator shows the specific capacities of 1495, 967, 808, 713, 601, and 408 mA h g^{-1} at the rates of 0.1, 0.2, 0.5, 1, 2, and 5 C, respectively. Furthermore, when the current density was turned back from 5 to 0.1 C, a discharge capacity could recover to 818 mA h g^{-1}, demonstrating an excellent rate performance. The battery with a small amount of electrolyte (25 μL) was also assembled, and the rate performance was studied as well (Figure S4a). Obviously, the battery assembled with the PAA separator still possesses an excellent rate performance with a high specific capacity of 416 mA h g^{-1} at a rate of 5 C. The overvoltage (ΔE) of the cell keeps a relatively low value of about 110 mV (Figure S4b).

The SEM images of the lithium anode before and after the rate test have been provided in Figure S5a−c. The Li surface with the PAA separator is almost smooth and flat after the rate test (Figure S5b). On the contrary, the Li surface with the Celgard separator is rough and seriously corroded (Figure S5c), indicating a serious diffusion of polysulfides. Furthermore, the corresponding EDS mapping of the lithium anode before and after the rate performance has also been detected. Compared to the case of the PAA separator (Figure S5d), a large amount of sulfur can be obviously observed to be evenly distributed over the entire surface of the lithium anode with the Celgard separator (Figure S5e), further indicating that the PAA separator can efficiently inhibit the "shuttle effect" of polysulfides and prevent the loss of the active material.

In general, the excellent electrochemical performance achieved for the cell assembled with the PAA separator is attributed to the following reasons. First, the surface of the PAA separator contains abundant negative ion-selective −COOH groups. These ion-selective groups could hamper the transport of the negative polysulfide, which prevents the loss of active sulfur materials. Second, the −COOH groups could create an electronegative surrounding which accelerates the transport of Li^+.[38] Therefore, it is difficult for the negative polysulfide to diffuse across the negative separator, whereas Li^+ could transport through it very easily. At the same time, −COOH groups on PAA separators are able to improve the wettability of the separator to liquid electrolyte, which is also very important to improve the lithium-ion-transfer properties of the batteries. Consequently, the −COOH groups on the PAA separator act as dual functions of suppressed "shuttle effect" of polysulfides and improved Li^+-transfer property.

At last, the electrochemical window stability is also very important for a separator material. Figure 7c represents the $I-V$ curves of PAA, PI, and Celgard separators. It can be observed that there is no electrochemical decomposition on the $I-V$ curve of the PAA separator below 4.5 V (vs Li^+/Li), indicating a remarkable electrochemical stability which could make the PAA separator with a potential application for high-voltage batteries.[39]

4. CONCLUSIONS

In summary, PAA nanofiber membranes with dual functions have been prepared by a facile electrospinning technique and applied as separators for L−S batteries. The PAA separator can not only effectively inhibit the "shuttle effect" of polysulfides but also promote the diffusion of Li^+. Especially, the −COOH groups allow rapid ion-transfer rate of positively charged Li^+ but prevent the diffusion of negatively charged polysulfide anions through the Coulombic interactions. Besides, the PAA separator possesses good thermal stability, high porosity, excellent electrolyte wettability, and remarkable electrolyte uptake. These advantages bring significant improvements in the battery performances, with a high initial discharge capacity of 1031 mA h g^{-1}, an excellent rate capability of 408 mA h g^{-1} at 5 C, and a good capacity retention of 781.8 mA h g^{-1} (76%) after 200 cycles at 0.2 C. In addition, the PAA separator needs no further imidization processes with low cost, being a very promising separator candidate for high-performance Li−S batteries.

■ ASSOCIATED CONTENT

Supporting Information

The Supporting Information is available free of charge on the ACS Publications website at DOI: 10.1021/acsami.8b10795.

SEM images of the PI separator at different magnifications; comparison of lithium-ion-transfer number of this work with the previous reports; elemental mappings of sulfur in the cathode before and after 100 cycles; rate capability and the discharge/charge profiles of the battery assembled by the PAA separator with a small amount of electrolyte; and SEM images of the lithium anode and the corresponding elemental mappings of sulfur before and after the rate performance with PAA and Celgard separators (PDF)

DOI: 10.1021/acsami.8b10795
ACS Appl. Mater. Interfaces 2018, 10, 42198−42206

AUTHOR INFORMATION

Corresponding Author

*E-mail: yuee_miao@dhu.edu.cn.

ORCID

Yue-E Miao: 0000-0002-3660-029X

Notes

The authors declare no competing financial interest.

ACKNOWLEDGMENTS

The authors are grateful for the financial support from the National Natural Science Foundation of China (21604010 and 51433001), the Fundamental Research Funds for the Central Universities (2232017D-01), the "Chenguang Program" supported by Shanghai Education Development Foundation and Shanghai Municipal Education Commission (16CG39), the Program of Shanghai Academic Research Leader (17XD1400100), and Shanghai Scientific and Technological Innovation Project (18JC1410600).

REFERENCES

(1) Geng, P.; Zheng, S.; Tang, H.; Zhu, R.; Zhang, L.; Cao, S.; Xue, H.; Pang, H. Transition Metal Sulfides Based on Graphene for Electrochemical Energy Storage. *Adv. Energy Mater.* **2018**, *8*, 1703259−1703284.

(2) Yin, Y.-X.; Xin, S.; Guo, Y.-G.; Wan, L.-J. Lithium-Sulfur Batteries: Electrochemistry, Materials, and Prospects. *Angew. Chem., Int. Ed.* **2013**, *52*, 13186−13200.

(3) Zheng, M.; Zhang, S.; Chen, S.; Lin, Z.; Pang, H.; Yu, Y. Activated Graphene with Tailored Pore Structure Parameters for Long Cycle-Life Lithium-Sulfur Batteries. *Nano Res.* **2017**, *10*, 4305−4317.

(4) Yang, Y.; Zheng, G.; Cui, Y. Nanostructured Sulfur Cathodes. *Chem. Soc. Rev.* **2013**, *42*, 3018−3032.

(5) Seh, Z. W.; Sun, Y.; Zhang, Q.; Cui, Y. Designing High-Energy Lithium-Sulfur Batteries. *Chem. Soc. Rev.* **2016**, *45*, 5605−5634.

(6) Xu, G.; Yan, Q.-b.; Wang, S.; Kushima, A.; Bai, P.; Liu, K.; Zhang, X.; Tang, Z.; Li, J. A Thin Multifunctional Coating on a Separator Improves the Cyclability and Safety of Lithium Sulfur Batteries. *Chem. Sci.* **2017**, *8*, 6619−6625.

(7) Shao, H.; Ai, F.; Wang, W.; Zhang, H.; Wang, A.; Feng, W.; Huang, Y. Crab Shell-Derived Nitrogen-Doped Micro-/Mesoporous Carbon as an Effective Separator Coating for High Energy Lithium-Sulfur Batteries. *J. Mater. Chem. A* **2017**, *5*, 19892−19900.

(8) Zhao, Y.; Liu, M.; Lv, W.; He, Y.-B.; Wang, C.; Yun, Q.; Li, B.; Kang, F.; Yang, Q.-H. Dense Coating of $Li_4Ti_5O_{12}$ and Graphene Mixture on the Separator to Produce Long Cycle Life of Lithium-Sulfur Battery. *Nano Energy* **2016**, *30*, 1−8.

(9) Lai, Y.; Wang, P.; Qin, F.; Xu, M.; Li, J.; Zhang, K.; Zhang, Z. A Carbon Nanofiber@Mesoporous δ-MnO_2 Nanosheet-Coated Separator for High-Performance Lithium-Sulfur Batteries. *Energy Storage Mater.* **2017**, *9*, 179−187.

(10) Cai, W.; Li, G.; Zhang, K.; Xiao, G.; Wang, C.; Ye, K.; Chen, Z.; Zhu, Y.; Qian, Y. Conductive Nanocrystalline Niobium Carbide as High-Efficiency Polysulfides Tamer for Lithium-Sulfur Batteries. *Adv. Funct. Mater.* **2018**, *28*, 1704865−1704875.

(11) Freitag, A.; Langklotz, U.; Rost, A.; Stamm, M.; Ionov, L. Ionically Conductive Polymer/Ceramic Separator for Lithium-Sulfur Batteries. *Energy Storage Mater.* **2017**, *9*, 105−111.

(12) Ma, G.; Huang, F.; Wen, Z.; Wang, Q.; Hong, X.; Jin, J.; Wu, X. Enhanced Performance of Lithium Sulfur Batteries with Conductive Polymer Modified Separators. *J. Mater. Chem. A* **2016**, *4*, 16968−16974.

(13) Zeng, P.; Huang, L.; Zhang, X.; Han, Y.; Chen, Y. Inhibiting Polysulfides Diffusion of Lithium-Sulfur Batteries Using an Acetylene Black-CoS_2 Modified Separator: Mechanism Research and Performance Improvement. *Appl. Surf. Sci.* **2018**, *427*, 242−252.

(14) Li, Y.; Zhu, J.; Zhu, P.; Yan, C.; Jia, H.; Kiyak, Y.; Zang, J.; He, J.; Dirican, M.; Zhang, X. Glass Fiber Separator Coated by Porous Carbon Nanofiber Derived from Immiscible PAN/PMMA for High-Performance Lithium-Sulfur Batteries. *J. Membr. Sci.* **2018**, *552*, 31−42.

(15) Li, Y.; Zhu, J.; Shi, R.; Dirican, M.; Zhu, P.; Yan, C.; Jia, H.; Zang, J.; He, J.; Zhang, X. Ultrafine and Polar ZrO_2-Inlaid Porous Nitrogen-Doped Carbon Nanofiber as Efficient Polysulfide Absorbent for High-Performance Lithium-Sulfur Batteries with Long Lifespan. *Chem. Eng. J.* **2018**, *349*, 376−387.

(16) Wang, P.; Zhang, Z.; Yan, X.; Xu, M.; Chen, Y.; Li, J.; Li, J.; Zhang, K.; Lai, Y. Pomegranate-like Microclusters Organized by Ultrafine Co Nanoparticles@Nitrogen-Doped Carbon Subunits as Sulfur Hosts for Long-life Lithium-Sulfur Batteries. *J. Mater. Chem. A* **2018**, *6*, 14178−14187.

(17) Huang, J.-Q.; Zhang, Q.; Peng, H.-J.; Liu, X.-Y.; Qian, W.-Z.; Wei, F. Ionic Shield for Polysulfides Towards Highly-Stable Lithium-Sulfur Batteries. *Energy Environ. Sci.* **2014**, *7*, 347−353.

(18) Lu, Y.; Gu, S.; Guo, J.; Rui, K.; Chen, C.; Zhang, S.; Jin, J.; Yang, J.; Wen, Z. Sulfonic Groups Originated Dual-Functional Interlayer for High Performance Lithium-Sulfur Battery. *ACS Appl. Mater. Interfaces* **2017**, *9*, 14878−14888.

(19) Lin, C.-E.; Zhang, H.; Song, Y.-Z.; Zhang, Y.; Yuan, J.-J.; Zhu, B.-K. Carboxylated Polyimide Separator with Excellent Lithium Ion Transport Properties for a High-Power Density Lithium-ion Battery. *J. Mater. Chem. A* **2018**, *6*, 991−998.

(20) Lee, J.; Lee, C.-L.; Park, K.; Kim, I.-D. Synthesis of an Al_2O_3-Coated Polyimide Nanofiber Mat and Its Electrochemical Characteristics as a Separator for Lithium Ion Batteries. *J. Power Sources* **2014**, *248*, 1211−1217.

(21) Wang, Q.; Song, W.-L.; Wang, L.; Song, Y.; Shi, Q.; Fan, L.-Z. Electrospun Polyimide-Based Fiber Membranes as Polymer Electrolytes for Lithium-ion Batteries. *Electrochim. Acta* **2014**, *132*, 538−544.

(22) Kong, L.; Yan, Y.; Qiu, Z.; Zhou, Z.; Hu, J. Robust Fluorinated Polyimide Nanofibers Membrane for High-Performance Lithium-ion Batteries. *J. Membr. Sci.* **2018**, *549*, 321−331.

(23) Wang, Y.; Wang, S.; Fang, J.; Ding, L.-X.; Wang, H. A Nano-Silica Modified Polyimide Nanofiber Separator with Enhanced Thermal and Wetting Properties for High Safety Lithium-ion Batteries. *J. Membr. Sci.* **2017**, *537*, 248−254.

(24) Zhang, H.; Lin, C.-E.; Zhou, M.-Y.; John, A. E.; Zhu, B.-K. High Thermal Resistance Polyimide Separators Prepared via Soluble Precursor and Non-Solvent Induced Phase Separation Process for Lithium Ion Batteries. *Electrochim. Acta* **2016**, *187*, 125−133.

(25) Dai, J.; Shi, C.; Li, C.; Shen, X.; Peng, L.; Wu, D.; Sun, D.; Zhang, P.; Zhao, J. A Rational Design of Separator with Substantially Enhanced Thermal Features for Lithium-ion Batteries by the Polydopamine-Ceramic Composite Modification of Polyolefin Membranes. *Energy Environ. Sci.* **2016**, *9*, 3252−3261.

(26) Zhang, Y.; Wang, Z.; Xiang, H.; Shi, P.; Wang, H. A Thin Inorganic Composite Separator for Lithium-ion Batteries. *J. Membr. Sci.* **2016**, *509*, 19−26.

(27) Ghazi, Z. A.; He, X.; Khattak, A. M.; Khan, N. A.; Liang, B.; Iqbal, A.; Wang, J.; Sin, H.; Li, L.; Tang, Z. MoS_2/Celgard Separator as Efficient Polysulfide Barrier for Long-Life Lithium−Sulfur Batteries. *Adv. Mater.* **2017**, *29*, 1606817−1606822.

(28) Duretz, T.; Petri, B.; Mohn, G.; Schmalholz, S. M.; Schenker, F. L.; Müntener, O. The Importance of Structural Softening for the Evolution and Architecture of Passive Margins. *Sci. Rep.* **2016**, *6*, 38704−38710.

(29) Han, E.; Wang, Y.; Chen, X.; Shang, G.; Yu, W.; Niu, H.; Qi, S.; Wu, D.; Jin, R. Consecutive Large-Scale Fabrication of Surface-Silvered Polyimide Fibers via an Integrated Direct Ion-Exchange Self-Metallization Strategy. *ACS Appl. Mater. Interfaces* **2013**, *5*, 4293−4301.

(30) Wu, K.; Hu, Y.; Shen, Z.; Chen, R.; He, X.; Cheng, Z.; Pan, P. Highly Efficient and Green Fabrication of a Modified C Nanofiber Interlayer for High-Performance Li-S Batteries. *J. Mater. Chem. A* **2018**, *6*, 2693−2699.

DOI: 10.1021/acsami.8b10795
ACS Appl. Mater. Interfaces 2018, 10, 42198−42206

(31) Barchasz, C.; Molton, F.; Duboc, C.; Leprêtre, J.-C.; Patoux, S.; Alloin, F. Lithium/Sulfur Cell Discharge Mechanism: An Original Approach for Intermediate Species Identification. *Anal. Chem.* **2012**, *84*, 3973−3980.
(32) Li, Y.; Zhan, H.; Liu, S.; Huang, K.; Zhou, Y. Electrochemical Properties of the Soluble Reduction Products in Rechargeable Li/S Battery. *J. Power Sources* **2010**, *195*, 2945−2949.
(33) Yoon, S.; Lee, Y.-H.; Shin, K.-H.; Cho, S. B.; Chung, W. J. Binary Sulfone/Ether-Based Electrolytes for Rechargeable Lithium-Sulfur Batteries. *Electrochim. Acta* **2014**, *145*, 170−176.
(34) Zhang, S.; Cao, J.; Shang, Y.; Wang, L.; He, X.; Li, J.; Zhao, P.; Wang, Y. Nanocomposite Polymer Membrane Derived from Nano TiO_2-PMMA and Glass Fiber Nonwoven: High Thermal Endurance and Cycle Stability in Lithium Ion Battery Applications. *J. Mater. Chem. A* **2015**, *3*, 17697−17703.
(35) Qin, X.; Wang, X.; Xie, J.; Wen, L. Hierarchically Porous and Conductive $LiFePO_4$ Bulk Electrode: Binder-Free and Ultrahigh Volumetric Capacity Li-ion Cathode. *J. Mater. Chem.* **2011**, *21*, 12444−12448.
(36) Ghazi, Z. A.; Zhu, L.; Wang, H.; Naeem, A.; Khattak, A. M.; Liang, B.; Khan, N. A.; Wei, Z.; Li, L.; Tang, Z. Efficient Polysulfide Chemisorption in Covalent Organic Frameworks for High-Performance Lithium-Sulfur Batteries. *Adv. Energy Mater.* **2016**, *6*, 1601250−1601255.
(37) Huang, J.-Q.; Zhuang, T.-Z.; Zhang, Q.; Peng, H.-J.; Chen, C.-M.; Wei, F. Permselective Graphene Oxide Membrane for Highly Stable and Anti-Self-Discharge Lithium-Sulfur Batteries. *ACS Nano* **2015**, *9*, 3002−3011.
(38) Yu, X.; Joseph, J.; Manthiram, A. Suppression of the Polysulfide-Shuttle Behavior in Li-S Batteries Through the Development of a Facile Functional Group on the Polypropylene Separator. *Mater. Horiz.* **2016**, *3*, 314−319.
(39) Li, H.; Chen, Y.-M.; Ma, X.-T.; Shi, J.-L.; Zhu, B.-K.; Zhu, L.-P. Gel polymer Electrolytes Based on Active PVDF Separator for Lithium Ion Battery. I: Preparation and Property of PVDF/Poly(dimethylsiloxane) Blending Membrane. *J. Membr. Sci.* **2011**, *379*, 397−402.

DOI: 10.1021/acsami.8b10795
ACS Appl. Mater. Interfaces 2018, 10, 42198−42206